La Metallurgia Italiana
International Journal of the Italian Association for Metallurgy

DOI 10.36146/2026_01_37

From kinetics to imagery: A JMAK-informed, chained predictive artificial intelligence method for interpretable steel microstructure simulation

S. Bazri, C. Mapelli, D. Mombelli, R. Nemfardi, R. Bedini, G. Zucchelli

This paper presents a novel, physically informed machine learning (ML) framework for the accurate modeling and visualization of steel microstructure evolution during annealing. Utilizing a chained support vector regression (SVR) architecture with optimized hyperparameters, the model sequentially predicts key microstructural states, ensuring metallurgical consistency. The process begins by forecasting recrystallization fraction (RF) kinetics, which is critically constrained by the classical Johnson–Mehl–Avrami–Kolmogorov (JMAK) model. The resulting JMAK-corrected RF then serves as a fundamental input to subsequent SVR models, which forecast the average grain size (AGS) and, finally, essential image-based microstructural features (mean and standard deviation of pixel intensity). This chained approach inherently prioritizes physically sound outputs, avoiding the consistency issues of isolated predictions. A unique visualization methodology is introduced, which selects and maps the closest experimental inverse pole figure (IPF) maps to the predicted states. This robust, multi-stage framework establishes a powerful, data-driven tool for simulating complex material evolution, thus minimizing the need for extensive experimental operations in materials design and process optimization.

KEYWORDS: MACHINE LEARNING, MICROSTRUCTURE, STEEL, SVR MODEL, JAMK, RECRYSTALLIZATION, MATERIALS DESIGN;

INTRODUCTION

The drive to accelerate materials design demands a shift from costly, time-consuming experimental programs to efficient, data-driven computational methods (Gupta et al., 2026). While ML has proven transformative across materials science, successfully predicting static properties such as strength and hardness, the accurate modeling of microstructure evolution during thermomechanical processing, which dictates the properties, remains a critical, unresolved challenge (Ghaffari Farid et al., 2025; Tiexu et al., 2024; Bruno et al., 2024). This challenge is rooted in the complex, sequential, and interdependent nature of phenomena like recrystallization (RX) and grain growth, where the progression of one state directly dictates the kinetics of the next (Bazri et al., 2023; Song et al., 2024).

Conventional ML models often fail in this domain because they treat microstructural features (like recrystallization fraction and grain size) as independent outputs, neglecting the inherent physical and kinetic laws (e.g., Avrami kinetics) that govern their relationship (SharafEldin et al., 2025; C. Wang et al., 2025; X. Wang et al., 2025; Gao et al., 2025). This results in "black-box" predictions that, while

Shahab Bazri, Carlo Mapelli, Davide Mombelli
Department of Mechanical Engineering, Politecnico di Milano, 20156 Milan, Italy

Renato Nemfardi, Roberto Bedini, Giorgio Zucchelli
Eure Inox srl, Via Leonardo Da Vinci, 2, 20068 Peschiera Borromeo MI, Italy

numerically accurate within the training domain, frequently yield physically inconsistent or unrealistic results when simulating the evolution over time or extrapolating to new conditions. A need exists for a robust framework that explicitly embeds metallurgical principles to ensure the physical integrity of its predictions (Lertkiatpeeti et al., 2024; Suzuki et al., 2024; Gupta et al., 2023).

This paper introduces a novel chained SVR-JMAK framework designed to overcome these limitations. The central hypothesis is that by integrating a classical JMAK kinetic constraint into a sequential SVR architecture, the predictions that are highly accurate, physically consistent, and fully interpretable would be achievable. The framework operates as a chain, where the JMAK-corrected prediction of RF acts as a critical, physically-informed input for the subsequent prediction of AGS and key image-based features. The unique contribution is further cemented by a visualization methodology, offering metallurgists a practical, powerful simulation tool for process optimization.

METHODS: COMPUTATIONAL FRAMEWORK

Dataset and feature engineering

The models were trained using a comprehensive dataset derived from annealing experiments on ferritic stainless steel (FSS), encompassing various annealing soaking temperatures (AST), annealing incubation times (AIT), and prior deformation conditions. The target microstructural features of RF, AGS, and image characteristics, were extracted from electron backscatter diffraction (EBSD) IPF maps. input features for the ML models included the processing parameters (AST, AIT) alongside measured prior state features such as the initial grain size. To be exact, the experimental dataset of the samples include different conditions, from the as-received specimen, 88C with RF of 0.1%, and (as the equivalent circular diameter also denoted by d) AGS of 58.24 μm, to different annealed states, including 50C (RF=2.96%, AGS=43.30 μm), 53C (RF=46.0%, AGS=32.36 μm), 55C (RF=74.9%, AGS=42.74 μm), 64C (RF=4.03%, AGS=48.16 μm), 67C (RF=60.0%, AGS=40.11 μm), 68C (RF=91.1%, AGS=41.81 μm), 78C (RF=9.3%, AGS=53.57 μm), 80C (RF=40.0%, AGS=38.45 μm), and 82C (RF=93.1%, AGS=45.98 μm). These specimens had undergone the AST values of 0.65, 0.68, and 0.71, as the homologous temperature (a temperature ratio between the annealing temperature over melting point (abbreviated as TRAM)) and within various AITs.

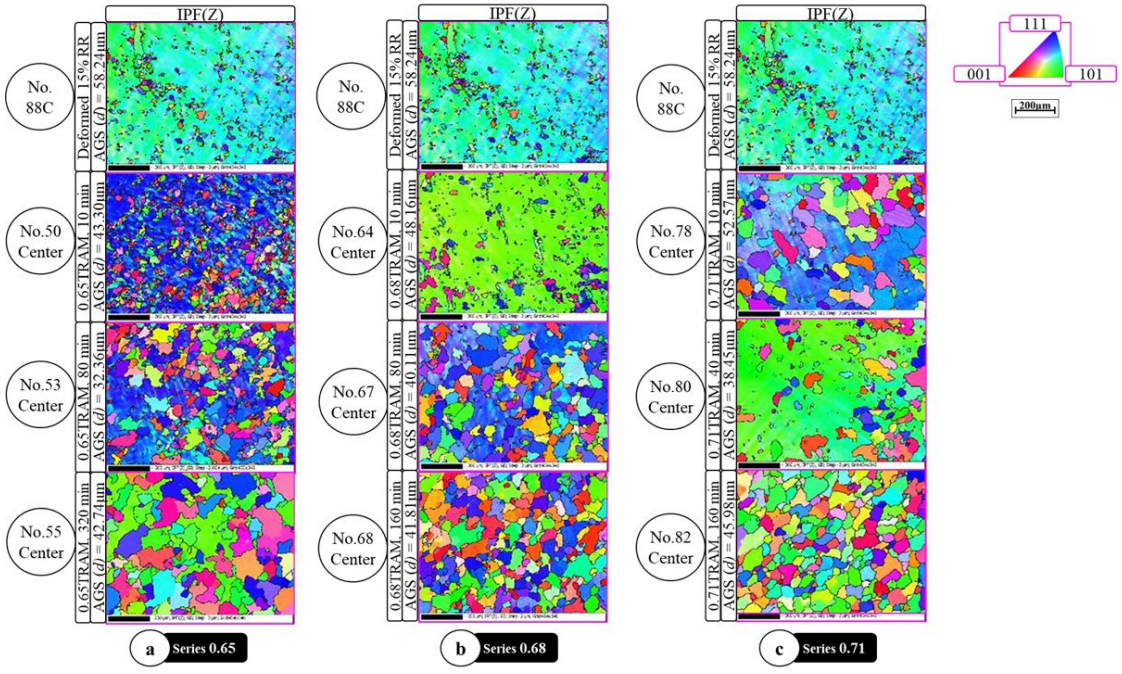

Fig.1 - Representative experimental IPF maps showcasing the microstructure evolution for different annealing conditions. Each series (a, b, c) corresponds to a different initial EBSD-post-processing calculated RF and displays the grain structure and AGS at various annealing times.

The chained SVR-JMAK prediction framework

To address the limitations of conventional ML models that ignore physical interdependencies, a chained SVR architecture, explicitly linking predictions across sequential stages of microstructural evolution, was employed. The SVR model, which utilizes a Gaussian (Radial basis function (RBF)) kernel, was selected for its robustness in handling complex, non-linear regression tasks on limited, high-dimensional materials datasets. The framework operates in a four-stage, sequential manner, as elaborated below and according to figure 1.

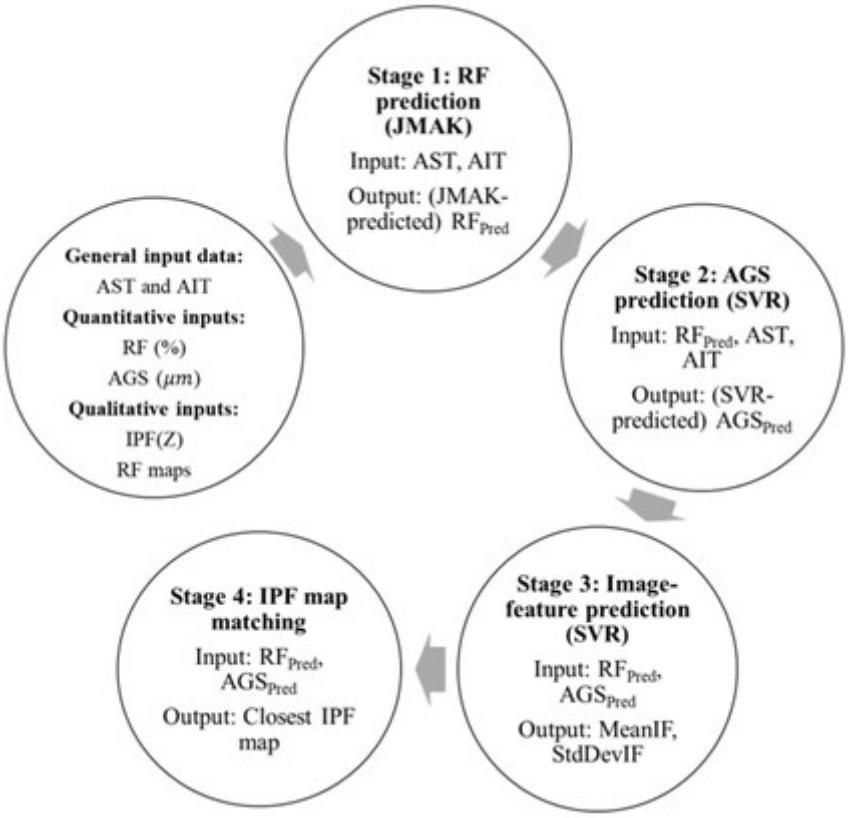

Fig.2 - Schematic representation of the chained SVR-JMAK framework for microstructure prediction and visualization.

As for stage 1 of the initial RF prediction (JMAK constraint), the JMAK kinetic model is employed first. Using the non-linear least squares method, the JMAK equation is fitted directly to the experimental RF data based on AIT and AST. This step ensures the RF prediction strictly adheres to known metallurgical transformation kinetics, guaranteeing physical consistency. The JMAK-modeled RF is the physically-consistent output of this first stage. Regarding stage 2 of AGS prediction, the JMAK-predicted RF is used as a critical, physically-informed and metallurgically-consistent input feature for the second SVR model. This SVR then predicts the AGS. This explicit link ensures that the predicted grain size is consistent with the predicted extent of recrystallization. About stage 3 and image feature prediction, the final stage of the SVR chain uses both the predicted RF and predicted AGS as inputs to forecast key image-based features of the microstructure, specifically the mean and standard deviation of pixel intensity. These numerical features serve as the critical proxy for the visual state of the microstructure. At stage 4 as the IPF map visualization and validation, the predicted image features from stage 3 are used to generate a visual representation of the final microstructure. This is achieved by searching the experimental dataset to identify the IPF

map whose measured features are numerically closest to the model's predictions.

Model optimization and hyperparameter tuning

All SVR models within the chain were subjected to a rigorous Bayesian optimization process. This approach efficiently searches the hyperparameter space (specifically the regularization parameter C, the kernel coefficient γ, and the epsilon parameter ϵ) to minimize the RMSE on a dedicated validation set. This systematic tuning ensures high prediction accuracy and optimal generalization capability for each stage.

RESULTS AND DISCUSSION

Predictive performance of the chained SVR framework

The sequential, chained architecture demonstrated exceptional performance in predicting the interdependent microstructural features. The rigorous Bayesian optimization ensured that each SVR model achieved optimal hyperparameters, leading to highly accurate predictions on the held-out test set. About the recrystallization kinetics through stage I, the JMAK-predicted model for RF kinetics achieved the highest predictive performance, with a correlation coefficient (R^2) consistently exceeding 0.97 and a low RMSE. This high accuracy validates the strategy of embedding a physical constraint (JMAK) within the ML architecture, resulting in physically sound evolution curves. The robust fit of the JMAK model to experimental data and its reliable extrapolation capabilities are further illustrated in Figure 3, which shows the predicted RF evolution over varying AITs for different initial recrystallization states (AST series). The solid lines represent the JMAK model's extrapolation, while the markers denote the original training data, confirming the model's ability to accurately capture and extend the kinetic trends.

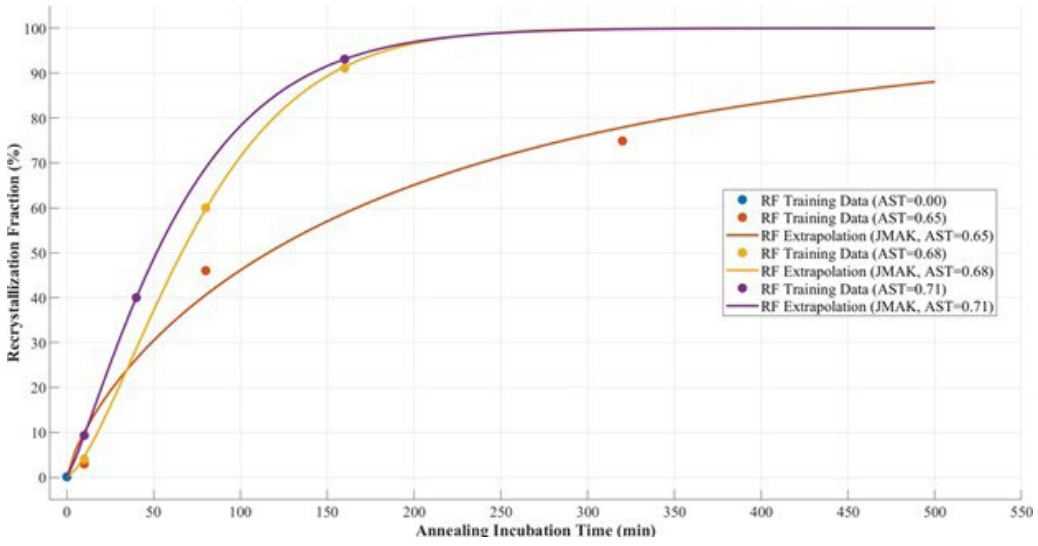

Fig.3 - Predicted RF evolution (JMAK).

Moreover, regarding the grain size prediction of stage II, the SVR model predicting AGS, which utilizes the predicted RF as a crucial input, also exhibited high fidelity, with R^2 values above 0.95. The success here confirms the ability of the chained approach to successfully transfer physically consistent information across stages, preventing the propagation of metallurgical inconsistencies. Figure 4 further supports this, presenting the SVR-predicted AGS evolution as a function of AIT. The curves illustrate the model's capacity to capture the complex, non-linear changes in grain size across different AST conditions, accurately reflecting the underlying microstructural phenomena. The agreement between the SVR extrapolation lines and the training data points highlights the model's strong predictive capability for AGS.

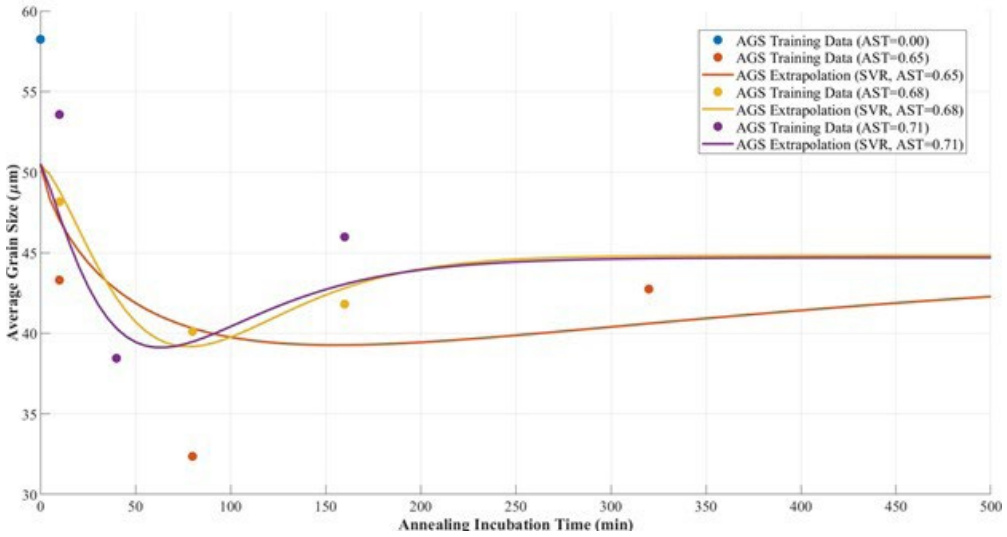

Fig.4 - Predicted AGS evolution from the SVR Model.

Via stage 3 of the image feature prediction, the final SVR models successfully mapped the predicted RF and AGS to the numerical image features (mean and standard deviation of pixel intensity), achieving high R^2 values (>0.94). This confirms the model's ability to numerically characterize the microstructural state, laying the foundation for accurate visual mapping. Figure 5 represents the SVR-predicted evolution of mean pixel intensity over AIT for various AST conditions. The accurate prediction of this image feature demonstrates the model's capability to capture subtle changes in the microstructure's visual characteristics, which are crucial for the subsequent visualization stage. The strong correlation between the predicted curves and experimental data points highlights the effectiveness of the chained SVR in characterizing complex image-based features.

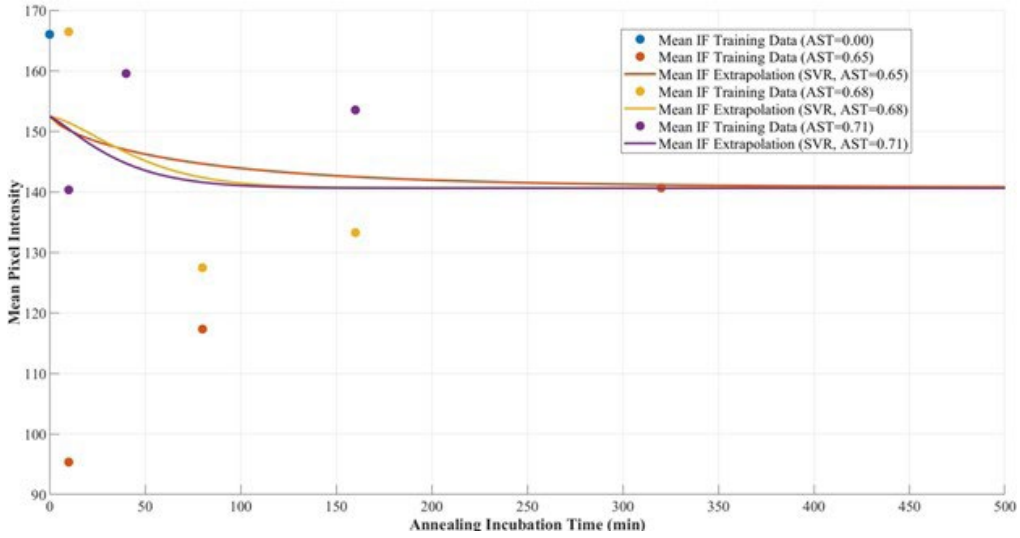

Fig.5 - SVR-predicted evolution of mean pixel intensity.

Likewise, figure 6 illustrates the SVR-predicted evolution of the standard deviation of pixel intensity as a function of AIT. The model accurately predicts the trends and magnitudes of spread in pixel intensity, further validating its capacity to capture comprehensive details of the microstructure's texture and heterogeneity. The consistency between the SVR extrapolations and training data points highlights the robustness of the chained approach in predicting complex image-derived features.

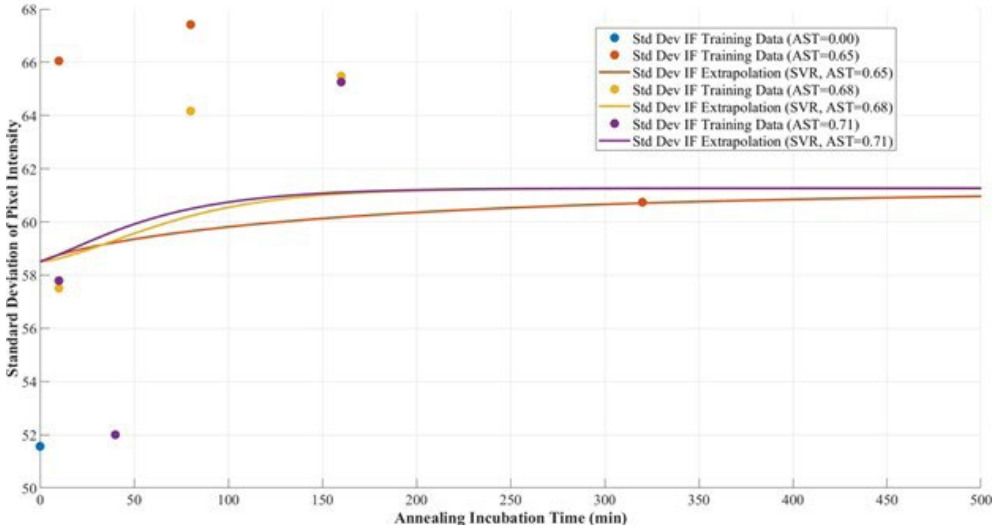

Fig.6 - SVR-predicted evolution of standard deviation of pixel intensity.

Interpretable visualization

The framework's interpretability is realized through the direct visualization of the predicted microstructural state, achieved by matching the numerical predictions to the closest experimental IPF map. This capability transforms the model's numerical outputs into a tangible, metallurgically relevant format, offering a clear visual proxy for the predicted microstructure. Figure 7 provides a compelling demonstration of this visualization capability, displaying examples of the predicted microstructures alongside their closest matching experimental IPF maps for specific annealing conditions. The close visual agreement between the model's predictions and the actual microstructures validates the framework's ability to accurately simulate and represent complex microstructural evolution.

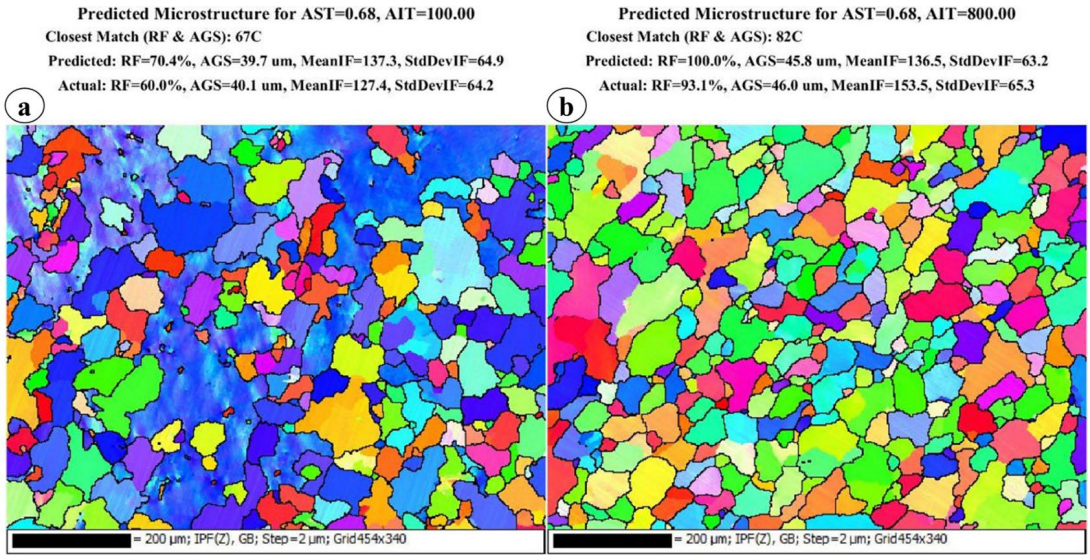

Fig.7 - Examples of predicted microstructures with their closest matching experimental IPF maps for different annealing conditions.

The core benefit of the chained SVR-JMAK architecture is the elimination of metallurgical inconsistencies that often cause independent-output ML models. By enforcing the sequential dependency and the JMAK modeling, the framework ensures that, for instance, a partially recrystallized state (low RF) will not simultaneously be associated with an unrealistically large grain size (high AGS), thereby yielding credible predictions across the entire processing window.

This inherent physical soundness establishes confidence in the framework's use for process optimization.

CONCLUSION

This study successfully developed and validated a novel ML-enabled, physically-constrained framework for predicting steel microstructure evolution. The core innovation lies in the chained SVR-JMAK architecture, which explicitly integrates metallurgical principles (JMAK kinetics) into a sequential prediction pipeline. The framework achieved superior predictive accuracy, with R^2 values exceeding 0.97 for key kinetic parameters, demonstrating that the integration of physical constraints and data-driven modeling leads to robust and metallurgically sound results. In conclusion, this research provides a powerful, data-driven alternative to extensive experimental testing and complex physical simulations, paving the way for efficient process optimization and accelerated materials design. Future work will focus on expanding the framework to predict mechanical properties and integrating it into a fully digital-twin simulation environment for various alloy systems.

DECLARATION OF COMPETING INTEREST

There are no conflicts of interest.

REFERENCES

[1] S. Bazri, C. Mapelli, S. Barella, A. Gruttadauria, D. Mombelli, R. Nemfardi, R. Bedini, G. Zucchelli. "Effect of cold drawing reduction rate on edge-to-center-characterized microstructure and orientation alongside residual stresses in conjunction with magnetic properties of low-carbon high-alloy ferromagnetic steel." Journal of Magnetism and Magnetic Materials, 591 (February 2024), 171699. https://doi.org/10.1016/j.jmmm.2023.171699

[2] F. Bruno, G. Konstantopoulos, G. Fiore, E. Rossi, M. Sebastiani, C. Charitidis, L. Belforte, M. Palumbo. "A novel machine learning method to exploit EBSD and nanoindentation for TRIP steels microstructures analysis." Materials and Design, 239 (March 2024), 112774. https://doi.org/10.1016/j.matdes.2024.112774

[3] D. Gao, Z. Shen, K. Chen, X. Zhou, H. Liu, J. Wang, Y. Li, Z. Liu, H. Deng, W. Y. Wang, X. Zeng. "Review of progress in calculation and simulation of high-temperature oxidation." Progress in Materials Science, 147 (January 2025), 101348. https://doi.org/10.1016/j.pmatsci.2024.101348

[4] M. Ghaffari Farid, H.R. Abedi, R. Ghasempour, A. Taylor, S. Khoddam, P.D. Hodgson. "Predicting the high-strain-rate deformation behavior and constructing processing maps of 304L stainless steel through machine learning and deep learning". Journal of Materials Research and Technology, 36 (May–June 2025), pp.7507–7518. https://doi.org/10.1016/j.jmrt.2025.05.009

[5] A. Kumar Gupta, S. Chakroborty, S. Kumar Ghosh, S. Ganguly. "A machine learning model for multi-class classification of quenched and partitioned steel microstructure type by the k-nearest neighbor algorithm". Computational Materials Science, 228 (September 2023), 112321. https://doi.org/10.1016/j.commatsci.2023.112321

[6] A. Kumar Gupta, S. Gupta, S. Kumar Ghosh, S. Ganguly. "Computer vision of ferrite, pearlite, austenite, bainite, and martensite: A deep learning framework toward high-throughput analysis of steel microstructure". Computational Materials Science, 261 (January 2026), 114319. https://doi.org/10.1016/j.commatsci.2025.114319

[7] K. Lertkiatpeeti, C. Janya-Anurak, V. Uthaisangsuk. "Effects of spatial microstructure characteristics on mechanical properties of dual phase steel by inverse analysis and machine learning approach". Computational Materials Science, 245 (October 2024), 113311. https://doi.org/10.1016/j.commatsci.2024.113311

[8] K. SharafEldin, B. D. Miller, W. Liu, J. Tischler, B. Anglin, A. El-Azab. "Informed unsupervised machine learning analysis of dislocation microstructure from high-resolution differential aperture X-ray structural microscopy data". Acta Materialia, 303 (January 2026), 121624. https://doi.org/10.1016/j.actamat.2025.121624

[9] K. Song, H. Ding, C. Zhang, L. Zhang, G. Deng, H. Zheng. "High-resolution simulating of grain substructure in cold rolling and its effects on primary recrystallization in annealing of ferritic stainless steel". Journal of Materials Research and Technology, 30 (May–June 2024), pp. 40–51. https://doi.org/10.1016/j.jmrt.2024.03.065

[10] M. Suzuki, K. Shizawa, M. Muramatsu. "Deep learning-aided inverse analysis framework to accelerate the exploration of DP steel microstructures". Materials Today Communications, 41 (December 2024), 110557. https://doi.org/10.1016/j.mtcomm.2024.110557

[11] P.Tiexu, Y. Haoyang, H. Jiaxin, F. Wei, L. Cong, Y. Zitong, Z. Xin, F. Jianhang, J. Puguang, X. Chaoqun, Y. Hui, Y. Fuxing. "Deciphering the composition-microstructure correlation in low-density FeMnAlC steels with machine learning". Computational Materials Science, 244 (September 2024), 113202. https://doi.org/10.1016/j.commatsci.2024.113202

[12] C. Wang, X. Wei, S. van der Zwaag, Q. Wang, W. Xu. "From creep-life prediction to ultra-creep-resistant steel design: An uncertainty-informed machine learning approach". Acta Materialia, 292 (June 2025), 121073. https://doi.org/10.1016/j.actamat.2025.121073

[13] X. Wang, F. Mao, X. Li, K. Miao, R. Shi, Y. Lin, C. Chen, C. Wang, H. Yu, S. Wei. "Machine learning-based prediction of microstructure and mechanical properties for 12Cr2Mo1V large cylindrical forgings". Materials Today Communications, 47 (July 2025), 112983. https://doi.org/10.1016/j.mtcomm.2025.112983